Oxid Met (2013) 79:303–311
DOI 10.1007/s11085-012-9332-4

ORIGINAL PAPER

Transient Oxidation of Cu-5at.%Ni(001): Temperature Dependent Sequential Oxide Formation

Yihong Kang · Langli Luo · Xiao Tong · David Starr · Guangwen Zhou · Judith C. Yang

Received: 17 April 2012 / Published online: 22 December 2012

Abstract The transient oxidation stage of a model metal alloy thin film was characterized with in situ ultra-high vacuum (UHV) transmission electron microscopy (TEM), X-ray photoelectron spectroscopy (XPS) and analytical high-resolution TEM. We observed the formations of nanosized NiO and Cu_2O islands when Cu-5at.%Ni(001) was exposed to oxygen partial pressure, $pO_2 = 1 \times 10^{-4}$ Torr and various temperatures in situ. At 350 °C epitaxial Cu_2O islands formed initially and then NiO islands appeared on the surface of the Cu_2O island, whereas at 550 °C NiO appeared first. XPS and TEM revealed a sequential formation of NiO and then Cu_2O islands at 550 °C. The temperature-dependent oxide selection may be due to an increase of the diffusivity of Ni in Cu with increasing temperature.

Y. Kang (✉)
Department of Mechanical Engineering and Materials Science, University of Pittsburgh, Pittsburgh, PA 15261, USA
e-mail: yik3@pitt.edu

L. Luo · G. Zhou
Department of Mechanical Engineering & Multidisciplinary Program in Materials Science and Engineering, State University of New York, Binghamton, NY 13902, USA
e-mail: langley821@gmail.com

G. Zhou
e-mail: gzhou@binghamton.edu

X. Tong · D. Starr
Brookhaven National Laboratory, Center for Functional Nanomaterials, Upton, NY 11973, USA
e-mail: xtong@bnl.gov

D. Starr
e-mail: dstarr@bnl.gov

J. C. Yang
Department of Chemical and Petroleum Engineering, University of Pittsburgh, Pittsburgh, PA 15261, USA
e-mail: judyyang@pitt.edu

Keywords Cu–Ni · Oxidation · In situ · TEM

Introduction

Wagner's theory can predict quite well oxide-scale evolution based on the relative amounts of the oxidizing components in a given binary alloy [1]. However, these descriptions of the oxide scale morphology are applicable for the later stages of oxide scale growth and are qualitative. These macroscopic depictions miss how initial surface conditions and early stages of oxidation lead to the final oxide scale morphology, though it is well-known that surface conditions and secondary elements dramatically impact the oxide structure. Visualizing the oxidation process at the nanometer scale with in situ experiments provides essential insights into the complex kinetics and energetics of the early stages of oxidation.

The general sequence of metal oxidation is oxygen chemisorption, nucleation and growth of oxide, and bulk oxide growth [2–13] In situ transmission electron microscopy (TEM) allows us to study the nucleation and growth processes of oxide at nanometer regime and below and bridges the gap between surface science studies and bulk oxidation or corrosion investigations. The dynamic information obtained from these in situ experiments enables us to understand and therefore manipulate the initial surface reactions that control the macroscopic scale morphologies.

Here, we report our initial oxidation results of a model metal alloys system, Cu-5at.%Ni(001), as an extension of our prior work of Cu and Cu–Au in situ oxidation [11, 13–20]Our extensive studies on Cu oxidation have demonstrated that oxidation involves nucleation and growth of oxide islands, surface diffusion and solid state reactions, and bears a striking resemblance to heteroepitaxy [11, 18]. Early-stage oxidation of both Cu and Ni has been extensively studied [18, 21–25] but little is known regarding the oxidation of Cu–Ni alloy. Cu–Ni alloys are expected to show more complex behavior, where the two components are 100 % solid-soluble down to $\sim$300 °C but Cu_2O and NiO show very limited miscibility. NiO, which has the cubic NaCl crystal structure with $a = 4.19$ Å, has a more negative standard free energy of formation than Cu_2O, which is simple cubic with $a = 4.26$ Å, and is expected to form more readily. In this case, depending on pO_2, either one or both components of the alloy will oxidize, thus enabling systematic determination of the effects of compositional and phase development during oxidation. Such insights into selective oxidation behavior of alloys are of significant importance since multiple elements are added to materials to provide optimal performance in an oxidizing environment.

Experimental Procedures

The microscope used in this work was a modified JEOL 200CX. A leak valve attached to the column of the microscope permits the introduction of gases directly into the microscope. In order to minimize the contamination, a UHV chamber was attached to the middle of the column, where the base pressure was less than

10^{-8} Torr without the use of the cryoshroud. The cryoshroud inside the microscope column can reduce the base pressure to approximately 10^{-9} Torr when filled with liquid helium. For more details about the experimental apparatus, see McDonald et al. [26].

Single crystal 80 nm thick Cu-5at.%Ni(001) thin films were created by simultaneous evaporation of 99.999 % pure Cu an Ni onto NaCl (001) substrates heated to 380 °C using Pascal dual-gun UHV e-beam evaporator. The films were removed from the substrate by dissolving the NaCl in de-ionized water, washed and then mounted on a top-entry TEM holder which can be resistively heated up to 1,000 °C in situ. Gas can be admitted into the column of the microscope through the leak valve from 5×10^{-5} to 760 Torr. The Cu-5at.%Ni(001) film formed a native oxide layer on the surface due to air exposure. Before oxidation in situ, the native oxide of Cu-5at.%Ni(001) film was reduced inside the TEM by annealing the Cu-5at.%Ni(001) films at 750 °C within an Ar plus 2 % H_2 gas mixture at a pressure of 5×10^{-4} Torr. To oxidize the Cu film, scientific grade oxygen gas (99.999 % purity) was introduced into the TEM chamber at a partial pressure of 5×10^{-4} Torr and temperatures between 350 and 700 °C. A Gatan SC1000 Orius^{TM} CCDcamera was used to capture the oxidation process in situ. *Ex situ* analytical TEM was conducted on a JEOL JEM 2100F, which is a 200 keV field-emission gun TEM/scanning TEM (STEM) equipped with an analytical pole-piece, Oxford energy dispersive X-ray spectroscopy (EDS) system, and a Gatan Tridium system for electron-energy loss-spectroscopy (EELS) and elemental mapping. This instrument is capable of 0.23 nm point resolution and 1 nm probe size for imaging and elemental analysis.

The XPS experiments were carried out in aUHV chamber equipped with an X-ray photoelectron spectrometer—SPECS Phoibos 100 MCD analyzer and an Ar^+ ion sputtering gun. The chamber typically has a base pressure of 2×10^{-10} Torr. A non-monochromatized Al-Kα X-ray source ($h\nu = 1{,}486.6$ eV) was used for the XPS studies. The sample was heated via a ceramic button heater and its temperature was monitored with a type-K thermocouple. The samples were annealed in the XPS chamber at 800 °C in H_2gas to remove the native oxide. Oxygen gas (purity = 99.9999 %) was introduced to the system through a variable pressure leak valve and the sample was oxidized under a controlled pO_2 under the same conditions as in situ TEM experiments.

Results and Discussion

Figure 1a is the bright field TEM image of the Cu-5at.%Ni(001) before H_2 exposure where the contrast could be due to strain from the native oxide. Figure 1c is the corresponding select area electron diffraction (SAED) pattern revealing the oxide formation where additional weak diffraction spots are due to the native oxide that formed during air exposure during the transport from the e-beam evaporator to the in situ UHV-TEM. After H_2 annealing in situ, the metal alloy film is smoother and the native oxide is removed (Fig. 1b, d).

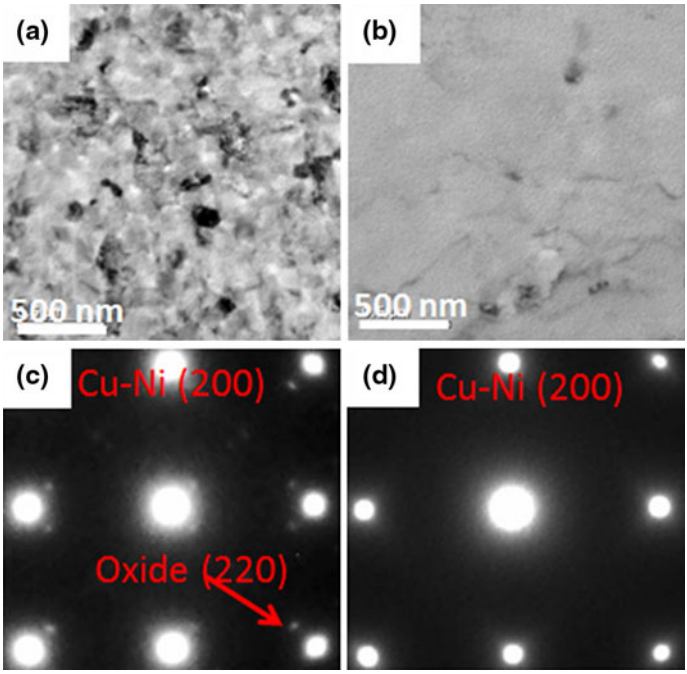

Fig. 1 Comparison of the Cu-5at.%Ni(001) before and after 1 h H_2 annealing at 750 °C and $pO_2 = 5 \times 10^{-4}$ Torr. **a** TEM bright field image showing the native oxide and strain contrast. **b** TEM bright field image showing the smooth and clean of the surface after annealing. **c** SAED pattern of (**a**) showing the existence of native oxide. **d** SAED pattern of (**c**) showing the removal of native oxide

For the XPS experiments, the Ni 2p peak was used to identify the formation of NiO due to the distinctive changes of the XPS spectrum (see Fig. 2a) [27]. Since Cu_2O and Cu have similar 2p XPS spectra, we focused on the Cu LMM Auger peak to identify Cu_2O, which has a 2 eV shift from metallic Cu (see Fig. 2b) [28, 29]. The Cu-5at.%Ni(001) films were also annealed in H_2 gas in the XPS chamber under the same conditions as the in situ UHV-TEM. The Fig. 2a, b show the clear shift of Ni 2p peak and Cu LMM peak obtained from the XPS system after hydrogen annealing, which also demonstrates the reduction of the native oxide to its metallic state.

Figure 3 compares the morphologies of oxide islands that formed during oxidation of Cu(001) to Cu-5at.%Ni(001) at various temperatures. Since Cu_2O has a simple cubic structure whereas NiO is face-centered cubic (fcc), the appearance of a (110) diffraction spots indicates Cu_2O formation. At 350 °C, epitaxial Cu_2O oxide islands with cube-on-cube orientation formed on the Cu-5at.%Ni(001) surface similar to Cu(001), but the morphology of the islands are polyhedral not triangular in cross section in comparison to Cu(001). At 550 °C, the appearance of the (220) diffraction spot without (110) diffraction spot indicates that NiO formed on the Cu–Ni surface not Cu_2O. Moreover, the epitaxial relationship between oxide and the film was observed to be NiO (111)//CuNi (001) and NiO (220)//CuNi(220), not

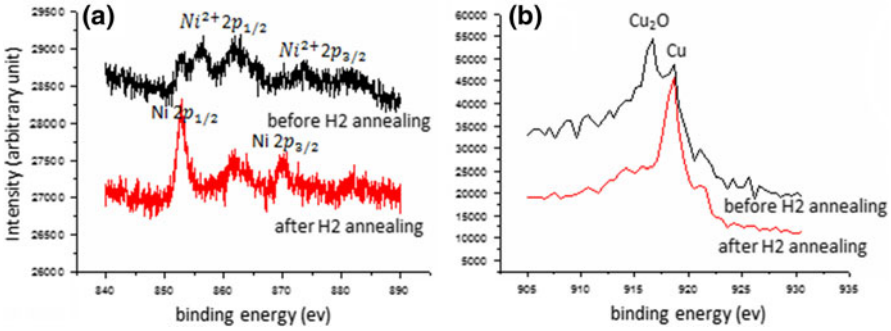

Fig. 2 XPS data of the Cu-5at.%Ni(001) before and after H_2 annealingfor 1 h at 550 °C. **a** The changes of Ni 2p peak after annealing indicating Ni oxides are reduced to Ni metal. **b** The shift of Cu LMM peak suggests reduction of the copper oxides to copper

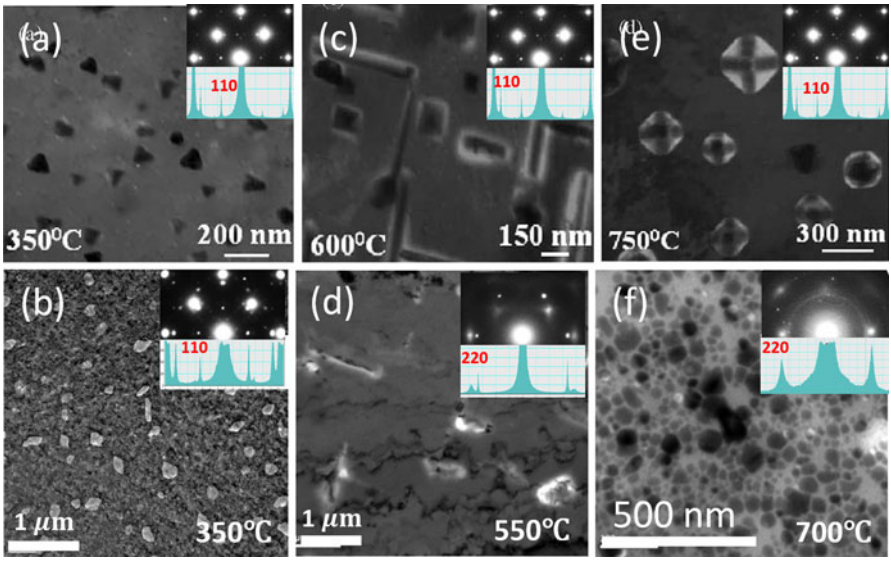

Fig. 3 Comparison of the oxide islands formed on Cu(001) and Cu-5at.%Ni(001) film under various temperatures and $pO_2 = 5 \times 10^{-4}$ Torr. The *insets* are the corresponding SAED pattern. The existence of (110) diffraction spots indicates the formation of Cu_2O, otherwise, NiO formed on the surface. **a** Triangular Cu_2O oxide islands formed on the Cu(001) surface at 350 °C. **b** Polyhedral oxide islands formed on the Cu-5at.%Ni(001) surface at 350 °C. **c** Rectangular and rod-like Cu_2O islands formed on the Cu(001) surface at 600 °C. **d** Polyhedral and rod-like NiO islands formed on the Cu-5at.%Ni(001) surface at 550 °C. **e** Cross-hatched Cu_2O islands formed on the Cu(001) surface at 750 °C. **f** Dense and round NiO islands formed on the Cu-5at.%Ni(001) surface at 700 °C

cube-on-cube (see the inset of Fig. 3d). At 700 °C, the oxide was identified as NiO but the islands are no longer epitaxial with respect to the Cu-5at.%Ni(001) film as evidenced by the SAED ring pattern. We have previously reported a change of epitaxy of Cu_2O islands as a function of oxidizing pressure [30]. Epitaxy is favored at low oxidizing pressures when the energy barrier to oxide nucleation is high and

supply of oxygen is low, whereas high oxygen pressure enhances rapid nucleation and the probability for randomly oriented oxide nuclei. Similarly, the higher temperatures may favor NiO formation that has a lower nucleation barrier than Cu_2O and thus results in non-epitaxial NiO nucleation.

Since Cu_2O and NiO have similar lattice parameters, distinguishing NiO from Cu_2O using electron diffraction is difficult. We used *ex situ* analytical TEM to detect nickel on the Cu_2O surface. Figure 4a is a bright field TEM image of a Cu_2O island where the small dark contrast suggests NiO; the dotted line indicates the position of the EDS line scan revealing Ni on the Cu_2O island (Fig. 4b). Figure 4c shows the Ni 2p XPS spectrum taken at 3 and 120 min oxygen exposure at 5×10^{-4} Torr O_2 and 350 °C, where a significant NiO peak is noted after 120 min. XPS confirmed that NiO forms at 350 °C after long oxidation times. The combination of the XPS and TEM results indicate that NiO exists on the surface of the Cu_2O shown in Fig. 4a. Similar oxide duplex has been reported previously for Cu–Ni, but with Cu on the top of NiO [31].

To further understand the sequential oxidation of NiO and Cu_2O, we examined the oxidation behavior of Cu-5at.%Ni(001) films at 550 °C by XPS and in situ UHV-TEM. Figure 5a shows the change of Ni 2p XPS spectrum during the oxidation at oxygen pressure of 5×10^{-4} Torr. Before oxidation, it shows the metallic Ni 2p pattern. Only after a very short oxygen exposure time of 3 min, the Ni 2p peak indicates NiO. The Cu LMM peak shown in Fig. 3b did not change after 3 min of oxidation. After 30 min of oxidation, the Cu LMM peak reveals a small hump indicative of Cu_2O revealing the formation of a small amount of Cu_2O.

The same experiment was performed in the in situ UHV-TEM. Figure 6 shows in situ sequential bright field TEM images of nucleation and growth of a NiO island. In comparison to Cu(001) oxidation under similar conditions [24], the nucleation and growth of oxide islands on Cu-5at.%Ni(001) film are significantly faster. The nucleation density of oxide islands on the Cu-5at.%Ni(001) surface is two orders of magnitude lower than that on the Cu(001) surface, the nucleation density of oxide islands on Cu(001) surface is approximately 40 μm^{-2} after 30 min oxidation, while the nucleation density of oxide islands on Cu-5at.%Ni(001) is only approximately 0.5 μm^{-2} under the same condition. The oxide islands that formed on the Cu-5at.%Ni(001) contain more defect and strain contrast in comparison to Cu(001);

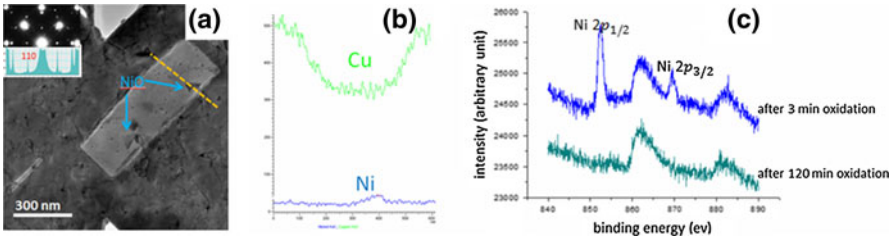

Fig. 4 **a** TEM bright field image of small NiO islands on a large Cu_2O island and corresponding electron diffraction pattern (*inset*). **b** Energy-dispersive X-ray spectroscopy (EDS) line-scan across a Cu_2O island where Ni is detected. **c** Ni 2p XPS data taken at 350 °C and $pO_2 = 5 \times 10^{-4}$ Torr as 3 and 120 min

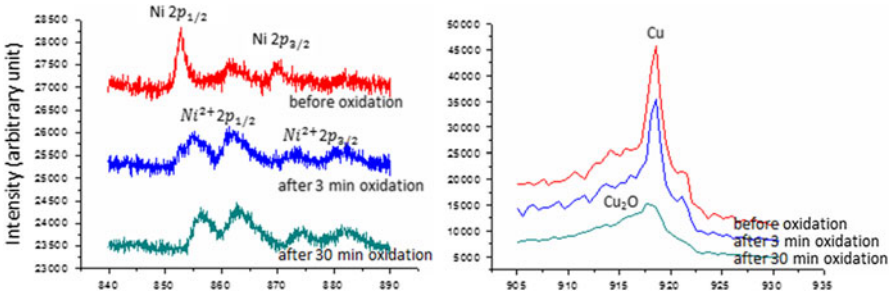

Fig. 5 Oxidation in XPS system under 550 °C and $pO_2 = 5 \times 10^{-4}$ Torr. **a** The change of Ni 2p peak after oxidation. **b** The change of Cu LMM peak after oxidation

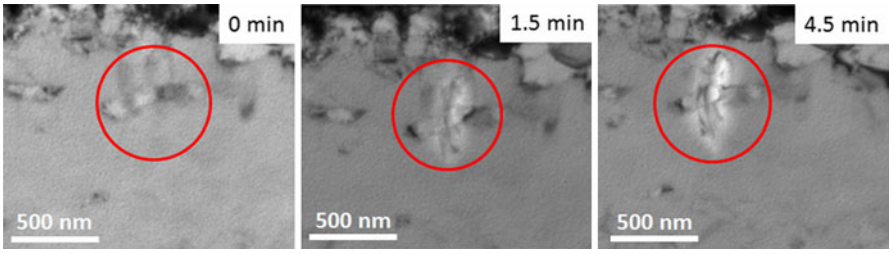

Fig. 6 In situ TEM observation of NiO island growth under 550 °C and $pO_2 = 1 \times 10^{-4}$ Torr. **a** Before oxidation. **b** After 1.5 min oxidation. **c** After 4.5 min oxidation

the oxide islands are polygon or irregular shape instead of rectangular shape observed during Cu(001) oxidation (see Fig. 3c, d).

Figure 7 compares the cross-sectional area growth of an NiO island, circled in Fig. 6, on the Cu-5at.%Ni(001) to Cu_2O island on Cu(001). The growth of the Cu_2O island on Cu(001) is due to oxygen surface diffusion [24]. However, the growth rate of the NiO island on Cu-5at.%Ni(001) is parabolic, indicating a bulk diffusion limited process for the oxide growth.

NiO is thermodynamically more stable than Cu_2O; it would be reasonable to expect NiO formation first. However, the in situ and *ex situ* TEM along with XPS experiments reveal a temperature dependant oxidation behavior for the initial oxide selection. We speculate that the temperature dependence of the Ni diffusion rate could explain the temperature dependent initial oxide selection. The diffusivities of Ni in Cu at various temperatures are displayed in Table 1 [32]. The diffusion length of Ni in Cu at 350 °C is only about 0.04 nm after 30 min, where Cu_2O islands form initially. Whereas at 550 °C where NiO islands form initially, the Ni diffusion length is comparable to the thickness of the Cu–Ni film. We speculate that at low temperatures, the Ni on the surface will oxidize quickly, but surface supply of Ni will deplete quickly and then Cu_2O will form rapidly. At higher temperature, the diffusion rate of Ni increases and its diffusion length becomes longer so that the supply of Ni to the alloy surface is plentiful and no longer limits the NiO growth.

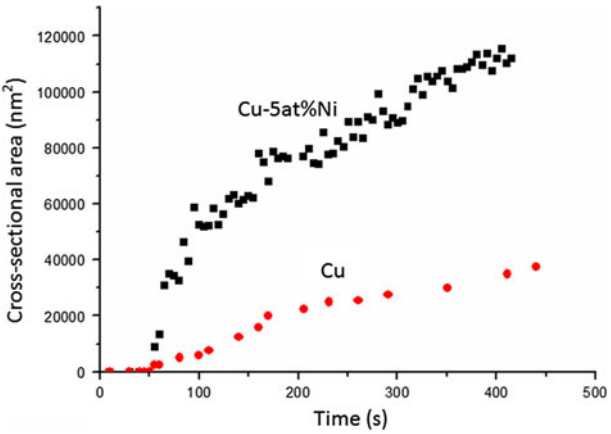

Fig. 7 The temporal evolution of the area of a NiO island formed on Cu-5at.%Ni (001) at 550 °C and $pO_2 = 1 \times 10^{-4}$ Torr, and comparison with a Cu_2O island formed on Cu (001) when the film was oxidized at 600 °C and $pO_2 = 1 \times 10^{-4}$ Torr

Table 1 Comparison of the diffusivity of Ni in Cu under 350, 550 and 700 °C

	350 °C	550 °C	700 °C
D $nm^2\ s^{-1}$	2×10^{-7}	2×10^{-2}	2
Time needed for the diffusion length reaches 40 nm (min)	3.3×10^{7}	3.3×10^{2}	3.3
Diffusion length for 30 min (nm)	0.04	12	120

Conclusions

The transient oxidation stage of Cu-5at.%Ni(001) was investigated by complementary in situ and *ex situ* TEM and XPS tools to identify the oxide formation and characterize their morphologies as function of oxidation time and temperature. Significant differences were noted between our earlier Cu(001) studies and the Cu-5at.%Ni alloys (001). A small increase of Ni content created a duplex NiO and Cu_2O islands. The selection of either NiO or Cu_2O to form initially depended on the oxidation temperature, which may be due to the temperature dependent diffusivity of Ni in Cu. Oxidation temperature also changed the epitaxy of the oxide islands from cube-on-cube to polycrystalline. The results here show the importance of temperature in controlling the microstructure of oxide during the oxidation. These observations of sequential and duplex oxide nucleation and growth may also apply to other alloys containing several oxidizing components owning to the interplay between the thermodynamic stabilities of various oxides and diffusivities of alloying elements.

Acknowledgments The authors thank M. France, L. Li and Z. Zhang for their assistance. This research program is supported by the National Science Foundation, Division of Materials Research (0706171). The *ex situ* TEM experiments were performed at Nanoscale Fabrication and Characterization Facility,

University of Pittsburgh. The XPS experiments were carried out at the Center for Functional Nanomaterials at Brookhaven National Laboratory, which is supported by the Department of Energy, Office of Basic Energy Sciences (DE-AC02-98CH10886).

References

1. C. Wagner, *Zeitschrift für Physikalische Chemie* **21**, 25–41 (1933).
2. P. H. Holloway and J. B. Hudson, *Surface Science* **43**, 123–140 (1974).
3. T. M. Christensen, C. Raoul and J. M. Blakely, *Applied Surface Science* **26**, 408 (1986).
4. I. Vaquila, M. Passeggi and J. Ferron, *Journal of Physics: Condensed Matter* **5**, A157 (1993).
5. H. M. Kennett and A. E. Lee, *Surface Science* **48**, 633 (1975).
6. H. Brune, J. Wintterlin, R. J. Behm and G. Ertl, *Physical Review Letters* **68**, 624 (1992).
7. J. Jacobsen, B. Hammer, K. W. Jacobsen and J. K. Nørskov, *Physical Review B* **52**, 14954 (1995).
8. W. H. Orr, Ph. D. Thesis (Cornell University, New York, 1962).
9. K. Thurmer, E. Williams and J. Reutt-Robey, *Science* **297**, 2033–2035 (2002).
10. J. C. Yang, B. Kolasa, J. M. Gibson and M. Yeadon, *Applied Physics Letters* **73**, 2841–2843 (1998).
11. J. C. Yang, M. Yeadon, B. Kolasa and J. M. Gibson, *Scripta Materialia* **38**(8), 1237–1242 (1998).
12. J. C. Yang and G. Zhou, Micron in press (2012).
13. G. W. Zhou, L. Wang, R. C. Birtcher, P. M. Baldo, J. E. Pearson, J. C. Yang and J. A. Eastman, *Physical Review Letters* **96**(22), 226108 (2006).
14. G. W. Zhou, W. S. Slaughter and J. C. Yang, *Physical Review Letters* **94**, 246101–246104 (2005).
15. G. W. Zhou and J. C. Yang, *Surface Science* **531**, 359–367 (2003).
16. G. Y. Zhou, C. Judith, *Journal of Material Research* **20**(7), 1684–1694 (2005).
17. J. C. Yang, L. Tropia and D. Evan, *Applied Physics Letters* **81**, 241–243 (2002).
18. J. C. Yang, M. Yeadon, B. Kolasa and J. M. Gibson, *Applied Physics Letters* **70**(26), 3522–3524 (1997).
19. J. C. Yang, M. Yeadon, B. Kolasa and J. M. Gibson, *MRS Bulletin* **481**, 557 (1997).
20. G. W. Zhou, L. Wang, R. C. Birtcher, P. M. Baldo, J. E. Pearson, J. C. Yang and J. A. Eastman, *Journal of Applied Physics* **101**, 033521–033526 (2007).
21. P. H. Holloway and J. B. Hudson, *Surface Science* **43**(1), 123–140 (1974).
22. P. H. Holloway and J. B. Hudson, *Surface Science* **43**(1), 141–149 (1974).
23. G. Zhou and J. C. Yang, *Applied Surface Science* **210**(3–4), 165–170 (2003).
24. G. Zhou and J. C. Yang, *Physical Review Letters* **89**(10), 106101 (2002).
25. G. Zhou, W. Slaughter and J. Yang, *Physical Review Letters* **94**(24), 246101 (2005).
26. M. L. McDonald, J. M. Gibson and F. C. Unterwald, *Review of Scientific Instruments* **60**, 700–707 (1989).
27. C. D. Wagner and G. E. Muilenberg, *Handbook of X-Ray Photoelectron Spectroscopy: A Reference Book of Standard Data for Use in X-Ray Photoelectron Spectroscopy*, (Physical Electronics Division, Perkin-Elmer Corporation, Eden Prairie, 1979).
28. S. Poulston, P. M. Parlett, P. Stone and M. Bowker, *Surface and Interface Analysis* **24**(12), 811–820 (1996).
29. L. E. Paul, *Journal of Electron Spectroscopy and Related Phenomena* **4**(3), 213–218 (1974).
30. L. Luo, Y. Kang, Z. Liu, J. C. Yang and G. Zhou, *Physical Review B: Condensed Matter* **83**(15), 155418 (2011).
31. G. Zhou, D. D. Fong, L. Wang, P. H. Fuoss, P. M. Baldo, L. J. Thompson and J. A. Eastman, *Physical Review B: Condensed Matter* **80**(13), 134106 (2009).
32. T. Van Dijk and E. J. Mittemeijer, *Thin Solid Films* **41**(2), 173–178 (1977).